Segmentation, Surface Extraction and Thickness Computation of Articular Cartilage

S. Kubilay Pakin[a], Jose G. Tamez-Pena[b], Saara Totterman[c], and Kevin J. Parker[d]

[a,b,d]University of Rochester, Electrical and Computer Engineering,
204 Hopeman Bldg., Rochester NY 14627 USA
[c]University of Rochester, Department of Radiology, Rochester NY USA

ABSTRACT

Accurate computation of the thickness of articular cartilage in 3D is crucial in diagnosis of joint diseases. The purpose of this research project is to develop an unsupervised method to produce three-dimensional (3D) thickness map of articular cartilage with magnetic resonance imaging (MRI). The method consists of two main parts, cartilage extraction and thickness map computation. The initial segmentation for cartilage extraction is achieved using a recently proposed algorithm which depends on region-growing. The regions produced during this process are labeled as cartilage or non-cartilage using a voting procedure which essentially depends on local 2-class clustering and makes use of prior knowledge about cartilage regions. Following cartilage extraction, femoral and tibial cartilages are separated by detecting the interface between them using a deformable model. After the separation, the cartilage surfaces are reconstructed as a triangular mesh and divided into two plates according to the relation between surface normal at each vertex and principal axes of the structure. For surface reconstruction, we propose an algorithm which incorporates a simple MR imaging model which allows surface representations with sub-voxel accuracy. Our thickness computation algorithm treats each plate separately as a deformable model while considering the other plate as the target surface towards which it is deformed. At the end of deformation, the thickness values at each vertex is defined as the distance between the locations at pre and post-deformation instances. The performance of the cartilage segmentation is compared to manual tracing. Also, the performance evaluation of the thickness computation algorithm on phantoms resulted in RMS errors on the order of 1%.

Keywords: Cartilage, segmentation, surface reconstruction, deformable models, thickness map

1. INTRODUCTION

One of the most common diseases that causes disability is Osteoarthritis (OA). OA results in thinning of cartilage. Thus, one needs methods to accurately obtain the thickness map of cartilage to diagnose and monitor the progression of the disease. Until this date, ample attempts have been made to achieve this goal using MRI which provides the capability of visualizing cartilage with good contrast.

The task of the computation of cartilage thickness is accomplished in two main steps. First, the cartilage is segmented from the 3D volume. Then, the thickness map of the cartilage, which is a 3D object, is constructed. Solloway et al. [1] use active shape models[2] to segment the cartilage. They compute the cartilage thickness by defining it as the distance between the points at which the line perpendicular to cartilage medial axis intersects the cartilage. However, both their segmentation and thickness computation is essentially 2D techniques. Especially, the computation of the thickness of a 3D object using a 2D technique is prone to generating significant errors since the latter does not take the orientation of cartilage into account. Eckstein et al. uses a region growing method to segment the cartilage.[3] Their method is a seeded region-growing approach in which the low contrast cartilage boundaries are manually marked to prevent misclassification. This is also a 2D method in which each slice of the volume is processed independently. Stammberger et al. employs B-spline snakes to each slice of the 3D volume.[4] The energy formulation of the snake they use has a coupling term, which depends on the shape of the segmented cartilage in

Further author information: (Send correspondence to S.K.P.)
S.K.P.: E-mail: pakin@ece.rochester.edu
J.T.P.: E-mail: pena@ece.rochester.edu
S.T.: E-mail: saaratotterman@urmc.rochester.edu
K.J.P.: E-mail: parker@ece.rochester.edu

the slice that is processed one step before. Thus, the 2D segmentations in each slice are not independent each other. They are correlated to the slice that is processed prior to them.

The last two techniques use the thickness computation algorithm proposed by Stammberger *et al.* .[5] It transforms the binary volume, which is constructed by cartilage segmentation, into a distance map using Eucledian Distance Transform (EDT). It also avoids using normal vectors defined on discrete surfaces.

The common problem of the segmentation techniques mentioned above is that they require user intervention either in the form of manual initialization or delineation of cartilage borders. The thickness computation algorithms have the drawback of working on the discrete grid. This fact makes it possible to come up with certain values only. This turns out to be especially important for a thin object such as cartilage. Our aim in this study to develop methods for automatic cartilage segmentation and thickness computation which will provide results with sub-pixel accuracy.

2. CARTILAGE SEGMENTATION

2.1. Initial Segmentation

The proposed method for cartilage segmentation is a region-based one in which the regions created in initial segmentation stage are assigned to two classes, cartilage or non-cartilage in the subsequent steps. Hence, it is crucial that the initial segmentation step provides a tessellation in which the regions consist of one class. The method can cope with over-segmentation but not under-segmentation due to its region-based nature. Because of these reasons, we utilized the segmentation algorithm proposed by Pena for initial segmentation stage.[6] The algorithm is based mainly on a region-growing scheme refined by region-splitting, region-merging and relaxation. It has been experimentally shown that, the algorithm provides good segmentation results for 3D MRI data.

The voting procedure, which will be covered in Section 2.2, uses the prior anatomical knowledge which states that the cartilage and bone tissues should be close to each other. In order to quantify this observation, we have to know which regions correspond to bone tissue. Specifically, we attempt to determine the regions that cover tibia and femur. This purpose is achieved by detecting the largest regions of tibia and femur using χ^2 statistic since the intensity profiles of both regions that are sought should bear a certain degree of similarity. Then the bone regions are completed by using a growing approach in which the local standard deviation profiles of bone regions are kept approximately unchanged.

2.2. Voting Procedure

The regions are labeled as cartilage or non-cartilage using the voting procedure proposed in Pakin *et al.* for segmentation of bone and soft tissue in digital radiographic images.[7] The voting procedure is essentially a 2-class local clustering of regions where the neighborhood system of each region is clustered into two classes using average intensity as feature (The neighborhood system of a region is defined as the region itself and the ones that are adjacent to it). It overcomes the difficulties which stem from the intensity inhomogeneities in medical images and the nonuniform intensity profiles of tissues to be segmented. The volume is also divided into sub-volumes using overlapping blocks to ensure local analysis.

Note that, clustering every neighborhood system implicitly assumes that both classes exist in every neighborhood system. This is clearly an invalid assumption. Let us call a neighborhood system *ambiguous* if it is a collection of regions which belong to one class. These systems have to be detected prior to clustering since some of the regions that belong to them will inevitably acquire incorrect votes as a result of clustering. The detection is based on the following assumption. *If a neighborhood system is ambiguous then the regions belong to it are non-cartilage regions.* This assumption is governed by the fact that the cartilage is a thin and highly localized tissue. Due to this reason, it is highly unlikely to have a cartilage region whose all adjacent regions are also cartilage. In this application, we used two different features to determine whether a neighborhood system contains at least one cartilage region or not.

The first measure used for this purpose, d_A, quantifies the closeness of a region, A, to the bones. It satisfies the following equation.

$$H_A(d_A) = 0.9N_A. \tag{1}$$

$H_A(d)$ is the cumulative distribution function of distances of voxels that belong to region A, to bone regions. Hence, $H_A(0)=0$ and $H_A(d)=N_A$ for $d > d_{A,max}$; $d_{A,max}$ is the distance between bone and the point of region A that is farthest away from bone. It is clear that computation of d_A, for all A, requires the knowledge of the distance between

bone region and each point in the volume that does not belong to bone. This is the definition of the Euclidian Distance Transformation (EDT) of the volume assuming the bone and the rest of the volume are background and foreground, respectively.[8] . For the computation of EDT, we chose to implement the technique proposed by Cuisenaire *et al.* which uses ordered propagation by bucket sorting.[9] Another issue regarding distance computation is the usage the physical distances as opposed to distances computed on the 3D grid. In 3D volumes, inter-slice resolution is usually greater than intra-slice resolution. Distance computation on the 3D grid without taking into account the inequality of inter and intra-slice resolutions introduces artifacts which adversely affects the performance of the algorithm. Due this fact, the distance between voxels i, and j, $d(i,j)$, is defined as:

$$d(i,j) = \left(r_x^2(i_x - j_x)^2 + r_y^2(i_y - j_y)^2 + r_z^2(i_z - j_z)^2 \right)^{1/2} , \qquad (2)$$

where r_x, r_y, and r_z are the resolutions in x, y, and z directions, respectively. The second measure used for the detection of ambiguous neighborhood systems is related to the contrast at the region boundaries and similar to the peripheral contrast concept proposed by Hojjetoleslami *et al.*[10] We define $\sigma_{A,brd}$ as the median value of the local standard deviation values along the border of region A. In other words, $\sigma_{A,brd} = \mathrm{Med}\{\mathcal{S}_{A,brd}\}$, where $\mathcal{S}_{A,brd} = \{\sigma(i)|i \in A, \exists j \; s.t \; j \notin A, j \in N_i, \forall i\}$. N_i and $\sigma(i)$ stands for the neighborhood of and the local standard deviation at voxel i, respectively.

The motivations behind these two features are obvious. The first feature is originated from the fact that the cartilage tissue is always close to bone tissue . Second feature is governed by a more qualitative observation which states that cartilage regions not only has high intensity but also boundaries along which there is good contrast, thus high local standard deviation. Hence, we argue that a cartilage region should possess relatively small d_A and large $\sigma_{A,brd}$ values. According to these definitions and observations, we state that a neighborhood system, $\mathcal{N}_{ik}$, is ambiguous if $d_{\mathcal{R}_{jik}} > \gamma_d$ and $\sigma_{\mathcal{R}_{jik},brd} < \gamma_\sigma, \forall \mathcal{R}_{jik}$.

The algorithm of the voting procedure is as follows:

ALGORITHM : VOTING PROCEDURE

For each $\mathcal{B}_k$
    For each $\mathcal{R}_{ik}$
        Compute the average intensities of $\{\mathcal{R}_{jik}\}$.
        If $\exists \mathcal{R}_{jik}$ such that $d_{\mathcal{R}_{jik}} < \gamma_d$ AND $\sigma_{\mathcal{R}_{jik},brd} > \gamma_\sigma$
            Cluster $\{\mathcal{R}_{jik}\}$ using k-means algorithm with 2 clusters.
            For each $\mathcal{R}_{jik}$
                If $\mathcal{L}_{jik}$ is cartilage, increment $\mathcal{V}(C)$ of corresponding $\mathcal{R}_m$.
                If $\mathcal{L}_{jik}$ is non-cartilage, increment $\mathcal{V}(NC)$ of corresponding $\mathcal{R}_m$.
            end
        Else
            For each $\mathcal{R}_{jik}$
                Increment $\mathcal{V}(NC)$ of corresponding $\mathcal{R}_m$.
            end
        end
    end
For each $\mathcal{R}_m$
    If $\mathcal{V}_m(C) > \mathcal{V}_m(NC)$, $\mathcal{R}_m$ is a cartilage region.
    If $\mathcal{V}_m(C) \leq \mathcal{V}_m(NC)$, $\mathcal{R}_m$ is NOT a cartilage region.
end

$\mathcal{R}_m$ is the mth region; $\mathcal{B}_k$ is the kth block; $\mathcal{R}_{ik}$ is the ith region in the kth block; $\mathcal{N}_{ik}$ is the neighborhood system of $\mathcal{R}_{ik}$, which is composed of $\mathcal{R}_{ik}$ and the regions that are adjacent to it; $\mathcal{R}_{jik}$ is the jth region in $\mathcal{N}_{ik}$; $\mathcal{L}_{jik}$ is the label of $\mathcal{R}_{jik}$ as the result of clustering of the regions in $\mathcal{N}_{ik}$; $\mathcal{V}_m(C)$ is the votes for cartilage label acquired by the mth region; $\mathcal{V}_m(NC)$ is the votes for non-cartilage label acquired by the mth region.

3. COMPUTATION OF CARTILAGE THICKNESS USING DEFORMABLE MODELS

The deformable model we employ for separation of tibial and femoral cartilages and thickness computation is a 3D model which consists of a triangular mesh. The formulation of 3D deformable models is an extension of classical formulation of snakes provided by Kaas et al. [11] and it is provided by Cohen et al. .[12]

The deformable model formulation we use in this study is similar to the work of Eviatar et al. .[13,14] Our deformable model consists of a surface mesh with triangular patches. We treat the deformable model as a collection of masses which are located at the node positions of the surface mesh. The nodes of the surface mesh are connected to each other with imaginary springs. The following notation will be kept throughout the sections which covers methods with deformable models:

N : Number of nodes in the mesh.

n_i : i^{th} node in the mesh, $i = 1 \cdots N$.

$\mathbf{p}_i = [p_{xi}\ p_{yi}\ p_{zi}]^T$: The coordinates of the ith node in 3D continuous space.

The energy of the deformable model which is denoted as $\mathcal{M}$ is equal to:

$$E(\mathcal{M}) = E_{ext}(\mathcal{M}) + E_{int}(\mathcal{M}) \tag{3}$$

where the internal energy $E_{int}(\mathcal{M})$ is definad as:

$$E_{int}(\mathcal{M}) = \frac{1}{2} \sum_{i=1}^{N} \sum_{j \in \mathcal{N}_i} k_{ij} \left((|p_{xi} - p_{xj}| - x_{0,ij})^2 + (|p_{yi} - p_{yj}| - y_{0,ij})^2 + (|p_{zi} - p_{zj}| - z_{0,ij})^2 \right). \tag{4}$$

In this formulation, $\mathcal{N}_i$ denotes the set of nodes that are adjacent to $\mathbf{p}_i$. It can alternatively be defined as $\mathcal{N}_i = \{j | \exists \mathcal{T} \text{ s.t. } \mathbf{p}_i \in \mathcal{T}, \mathbf{p}_j \in \mathcal{T}\}$, where $\mathcal{T}$ is a triangle in the surface mesh which is defined as the ordered list of its three vertices, $\mathcal{T} = (\mathbf{p}_k, \mathbf{p}_l, \mathbf{p}_m)$.[15] Also,

$$\mathbf{p}_{0,ij} = [x_{0,ij}\ y_{0,ij}\ z_{0,ij}]^T = [|p_{xi}^0 - p_{xj}^0|\ |p_{yi}^0 - p_{yj}^0|\ |p_{zi}^0 - p_{zj}^0|]^T \tag{5}$$

where $\mathbf{p}_i^0 = [p_{xi}^0\ p_{yi}^0\ p_{zi}^0]^T$ is the initial location of the ith node prior to the deformation.

The internal energy term tries to keep the distances between nodes as close to their initial values as possible. It is clear from the Eqn 4 is that any deviation from the initial distances between two adjacent nodes in any direction increases the overall internal energy. Another characteristic of the deformable model formulation is that the internal energy depends only on the scalar distance. In other words, The factor that is contributed to overall internal energy by the ith and j^{th} nodes remains unchanged unless the distance between them changes regardless of the direction of the vector $\mathbf{p}_i - \mathbf{p}_j$. This means that the formulation does not attempt to prevent bending of the deformable model even though it is possible to do so by incorporating second order neighbors to the energy expression. However, we believe that the performance gain for the applications in which we are interested will be minimal compared to the complexity of formulation and computation introduced by such an addition. The formulation of the model is concluded by the specification of the external energy, $E_{ext}(\mathcal{M})$. The external energy formulation will be provided in the incoming sections which covers separation of tibial and femoral cartilages and thickness computation since they require slightly altered external energy terms and different energy minimization methods.

3.1. Surface Mesh Generation

This section presents the algorithm used for the cartilage surface extraction. The algorithm incorporates a simple MR imaging model which allows surface representations with sub-voxel accuracy.

Although Marching-cubes type algorithms[16] can be used to extract the iso-surfaces from the raw data, they assume a simple sampling of a continuous distribution of the intensity profile. This continuity and sampling assumptions make marching-cubes unsuitable for the extraction of surfaces from MR data. First, human anatomy is a set of tissues with different MR properties; therefore, there are intensity discontinuities between tissues. Second, the MR imaging formation is an integration of the magnetic resonance properties, which makes signal intensity formation at boundaries dependent of the sampling point location..[17]

To overcome the difficulties associated with marching-cubes algorithms, we divided the problem of surface extraction it two steps: Raw surface extraction and surface correction. The raw surface extraction creates a simple surface representation of the tissue. The simple representation allows the correction of the surface nodes to the location that will recreate the raw data assuming simple MR formation model. Next, we describe in detail the two step approach.
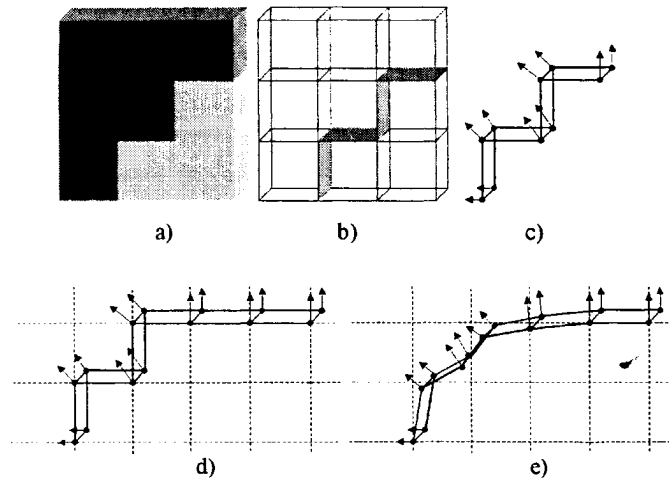
Figure 1. a)Single slice representation of the voxel classification into two different tissues. b)Surface generation from the voxel's faces at boundries c)Surface nodes and normal extracted from the face boundaries. d)Surface nodes and normals from the raw surface extraction e)Surface nodes and surface normals afer the node correction.

3.1.1. Raw surface extraction

At this point we assume that all the voxels in the volume have been classified as cartilage and non-cartilage tissue with high accuracy. We use a simple cube representation of each voxel in the image. Then the raw-surface is the set of every single square face that lies at the border between tissues. At each node point, $\mathbf{p}$, of the surface representation, the normal, $\mathbf{n_p}$, is also computed. The normal computation is done by averaging the normal of each face, v, attached to that point.

$$\mathbf{n_p} = c \sum_{v \in C} \mathbf{n}_v, \tag{6}$$

where C is the set of faces associated to the point $\mathbf{p}$, $\mathbf{n}_v$ is the normal at face v, and c is the normalization constant. Figure 1 shows the raw surface extraction process. This extraction process is very simple and yields simple surfaces composed by the set of square polygons.

3.1.2. Surface correction

The type of surfaces generated by the raw extraction algorithm are not adequate for estimation of cartilage thickness. The nodes of each surface are not in the right location. The next step is to place the surface nodes at the positions that will create the most accurate 3D reconstruction of the object.

We assume that the signal f at each voxel is the integration of the MR properties of the imaging volume:

$$f(i,j,k) = \int_{x,y,z \in \mathcal{R}} t(x,y,x), \tag{7}$$

where $f(i,j,k)$ is the observed value at discrete point (i,j,k), $t(x,y,z)$ is a piece-wise representation of the MR properties from the subject, and $\mathcal{R}$ is a spherical region around point (x,y,z).

The spherical region and the piece-wise model allows the implementation of a simple method for correcting the surface node locations. If we assume a two tissue model then the signal mixture at the boundary point $\mathbf{p}$ can go from 0% to 100%

$$f_{\mathbf{p}} = \alpha t_{\mathbf{p}}^a + (1 - \alpha) t_{\mathbf{p}}^b, \tag{8}$$

where α is the mixture of tissue signal inside the object, t^a, and $(1 - \alpha)$ is the amount of mixture from the tissue outside the object, t_b. The mixture, α, can be easily found if the local $t_{\mathbf{p}}^a$ and $t_{\mathbf{p}}^b$ values are known. These values are unknown; but local estimations can be obtain by using all the local non-boundary voxels. The signal estimation from the tissue inside the object is:

$$\hat{t}_{\mathbf{p}}^a = c_t \sum_{x=-1}^{1} \sum_{y=-1}^{1} \sum_{z=-1}^{1} f(i + x + n_x^p, j + y + n_y^p, k + z + n_z^p) s(i + x + n_x^p, j + y + n_y^p, k + z + n_z^p), \tag{9}$$

where (n_x^p, n_y^p, n_z^p) are the components of the normal $\mathbf{n_p}$ associated to the boundary node $\mathbf{p}$, whose original location is at the $point(i,j,k)$, c_t is the normalization constant, and $s(i,j,k)$ is the tissue classification map. Once $t_\mathbf{p}^a$ and $t_\mathbf{p}^b$ are known, then from 8:

$$\alpha = \frac{(f_\mathbf{p} - t_\mathbf{p}^b)}{(t_\mathbf{p}^a - t_\mathbf{p}^b)} \tag{10}$$

The signal value $f_\mathbf{p}$ is undefined because the point is at the voxel boundary. We select two possible values, one just next inside the tissue $f_\mathbf{p}^a$, and the other just outside the tissue $f_\mathbf{p}^b$. The signal value which is closest to the tissue value t^a or t^b is assumed to be a pure signal from that tissue. The other value is assumed to be a mixture. The mixture value is the one used in equation 10.

This mixture value is then used to adjust the node point coordinates along its normal. The amount of correction will depend on the assumptions made on the tissue boundary location. To simplify the equations, we approximate the tissue boundary as a simple plane. The plane assumption and a simple imaging volume model can be used to estimate the amount of correction. If the highest value difference is given by $f_\mathbf{p}^a$ the correction is:

$$\mathbf{p}^+ = \{p_x - (1-\alpha)n_x^p, p_y - (1-\alpha)n_y^p, p_z - (1-\alpha)n_z^p\} \tag{11}$$

On the other hand, if the highest value difference is given by $f_\mathbf{p}^b$ then the correction is:

$$\mathbf{p}^+ = \{p_x + \alpha n_x^p, p_y + \alpha n_y^p, p_z + \alpha n_z^p\} \tag{12}$$

This simple correction scheme will adjust the boundary points $\mathbf{p}$ to it new value $\mathbf{p}+$ according to the signal mixture very accurate in most low curvature regions. The correction will have some errors at high curvature points and points where three or more tissue are presents. This cases are not very common in most cartilage images. Therefore, the reconstructed surfaces from the corrected points are quite accurate.

3.2. Separation of Tibial and Femoral Cartilage and Segmentation Improvement

Following the cartilage segmentation, tibial and femoral cartilages have to be separated from each other in order to proceed with the computation of their thickness. We utilize two deformable models for this purpose. The initial locations of deformable models are femur-cartilage and tibia-cartilage interfaces. They are denoted as $\mathcal{M}_{fm}$ and $\mathcal{M}_{tb}$, respectively. Both meshes are deformed towards their respective target surfaces which are the sources of external energy. For $\mathcal{M}_{fm}$ and $\mathcal{M}_{tb}$, the target surfaces are the cartilage boundary except femur-cartilage and tibia-cartilage interfaces, respectively.

The external energy term in this framework depends on the distance between the nodes and the target surface. First, the EDT assuming the target surface and the rest of the volume as foreground and background, respectively, is computed. The value of the external energy at the location of node n_i is equal to the square of the distance of n_i to the target surface which is computed by bilinear interpolation and denoted by $d(\mathbf{p}_i)$. (Recall that, the distances on the volume grid are already computed by EDT.) Thus the external energy of the deformable model is equal to

$$E_{ext}(\mathcal{M}) = \sum_{i=1}^{N} d^2(\mathbf{p}_i) \tag{13}$$

The direct minimization of the total energy of the deformable surface is a difficult and computationally burdensome task. Thus, a greedy algorithm is applied to solve the minimization problem by opting for a suboptimal solution. The concept of the greedy algorithm we use is similar to the algorithm proposed by Williams $et\ al.$.[18] The algorithm finds the minimum of the energy term that is contributed to the total energy of the deformable mesh by each node assuming the other node locations are constant. The energy term contributed by the node n_i can be written as

$$E(n_i) = d^2(\mathbf{p}_i) + \sum_{j\in\mathcal{N}_i} k_{ij}\left((|p_{xi}-p_{xj}|-x_{0,ij})^2 + (|p_{yi}-p_{yj}|-y_{0,ij})^2 + (|p_{zi}-p_{zj}|-z_{0,ij})^2\right) \tag{14}$$

We used Powell's method for solving the minimization problem $\mathbf{p}_i = \arg\min_{\mathbf{p}_i}\{E(n_i)\}$.[19] The algorithm makes the implicit assumption that the thickness of femoral cartilage does not show abrupt changes. Forcing the deformable

surface to keep its surface area close to its initial value along with this assumption enables us to correctly detect the interface between femoral and tibial cartilages.

The algorithms utilized for cartilage segmentation up to this point were region-based techniques. Despite their advantages, when the regions are grouped under labels, they might cause tessellations with non-smooth boundaries. In order to create cartilage regions with smooth boundaries, the algorithm used for separation of tibial and femoral cartilages is utilized for improvement of cartilage segmentation. The underlying idea is to use the shape preserving property of deformable models for creating smooth cartilage borders. Since there are no other tissues between cartilage and bones (femur and tibia), the acquisition of smooth bone-cartilage interface results are more straightforward than the interface between cartilage and non-bone regions. The cartilage-non-bone interface is more prone to errors. The modification of cartilage segmentation and separation of tibial and femoral cartilages are achieved simultaneously by using two deformable models which are located at femur-cartilge and tibia-cartilage interfaces initially. The following notation is introduced to state the algorithm: $\mathcal{M}_{fm}$: The surface mesh at the femur-cartilage interface

$\mathcal{M}_{tb}$: The surface mesh at the tibia-cartilage interface

$n_{fm,i}$: i^{th} node of $\mathcal{M}_{fm}$ whose location is $\mathbf{p}_{fm,i} = [p_{fm,xi}\ p_{fm,yi}\ p_{fm,zi}]^{T}$

$n_{tb,i}$: i^{th} node of $\mathcal{M}_{tb}$ whose location is $\mathbf{p}_{tb,i} = [p_{tb,xi}\ p_{tb,yi}\ p_{tb,zi}]^{T}$

$d_{t,fm}(\mathbf{x})$: EDT of the volume assuming the target surface and the rest of the volume as foreground and background, respectively. Target surface is the boundary of the cartilage region except the femur-cartilage interface.

$d_{t,tb}(\mathbf{x})$: EDT of the volume assuming the target surface and the rest of the volume as foreground and background, respectively. Target surface is the boundary of the cartilage region except the tibia-cartilage interface.

$\mathbf{p}_{fm}$: The center of mass of femur region.

$\mathbf{p}_{tb}$: The center of mass of tibia region.

$\mathcal{T}_{fm,j}$: The jth triangular patch of the surface mesh $\mathcal{M}_{fm}$

$\mathcal{T}_{tb,j}$: The jth triangular patch of the surface mesh $\mathcal{M}_{tb}$

The algorithm can be stated as follows:

1. Construct $\mathcal{M}_{fm}$ and $\mathcal{M}_{tb}$.

2. Compute $d_{t,fm}(\mathbf{x})$ and $d_{t,tb}(\mathbf{x})$.

3. Deform $\mathcal{M}_{fm}$ and $\mathcal{M}_{tb}$ using the algorithm for deformation of surface mesh and appropriate target surfaces

4. Label the cartilage voxels as follows:

   Compute $\mathbf{p}_{fm}$, $\mathbf{p}_{tb}$

   for $\forall i \in \mathcal{C}$

     Construct $|\mathbf{p}_{fm}\mathbf{p}_{\mathcal{C},i}|$, $|\mathbf{p}_{tb}\mathbf{p}_{\mathcal{C},i}|$

       Case 1 : If $\exists \mathcal{T}_{fm,j}$ such that $|\mathbf{p}_{fm}\mathbf{p}_{\mathcal{C},i}|$ intersects $\mathcal{T}_{fm,j}$ AND

         if $\not\exists \mathcal{T}_{tb,j}$ such that $|\mathbf{p}_{tb}\mathbf{p}_{\mathcal{C},i}|$ intersects $\mathcal{T}_{tb,j}$

           $i \in \mathcal{C}_{tb}$

       Case 2 : If $\exists \mathcal{T}_{tb,j}$ such that $|\mathbf{p}_{tb}\mathbf{p}_{\mathcal{C},i}|$ intersects $\mathcal{T}_{tb,j}$ AND

         if $\not\exists \mathcal{T}_{fm,j}$ such that $|\mathbf{p}_{fm}\mathbf{p}_{\mathcal{C},i}|$ intersects $\mathcal{T}_{fm,j}$

           $i \in \mathcal{C}_{fm}$

       Case 3 : If $\not\exists \mathcal{T}_{fm,j}$ such that $|\mathbf{p}_{fm}\mathbf{p}_{\mathcal{C},i}|$ intersects $\mathcal{T}_{fm,j}$ AND

         if $\not\exists \mathcal{T}_{tb,j}$ such that $|\mathbf{p}_{tb}\mathbf{p}_{\mathcal{C},i}|$ intersects $\mathcal{T}_{tb,j}$

           $i \in \mathcal{C}_{fm}$

       Case 4 : If $\exists \mathcal{T}_{fm,j}$ such that $|\mathbf{p}_{fm}\mathbf{p}_{\mathcal{C},i}|$ intersects $\mathcal{T}_{fm,j}$ AND

         if $\exists \mathcal{T}_{tb,j}$ such that $|\mathbf{p}_{tb}\mathbf{p}_{\mathcal{C},i}|$ intersects $\mathcal{T}_{tb,j}$

           $i \notin \mathcal{C}$

   end

The algorithm can be seen as an extended version of the algorithm for cartilage voxel labeling stated earlier. Two deformable models are used for better separation performance. For a cartilage voxel, i, to be classified as femoral (tibial) cartilage, $\mathcal{M}_{tb}$ ($\mathcal{M}_{fm}$) has to be between tibia (femur) and i, and i has to between $\mathcal{M}_{fm}$ ($\mathcal{M}_{tb}$) and femur

(tibia). As a matter of fact, in the pseudo-code provided above, case 1 (2) correspond to this situation. Since the deformations of $\mathcal{M}_{fm}$ and $\mathcal{M}_{tb}$ are accomplished independently, they might intersect each other at the end. In such a situation, the labels of cartilage voxels that are swept by both deformable models are determined using $\mathcal{M}_{fm}$. Case 3 is the implementation of this method. The improvement of cartilage segmentation is achieved by excluding the cartilage voxels, which are not swept by neither deformable models, from $\mathcal{C}$. This modification (which corresponds to case 4) effectively approximates the tibial and femoral cartilage boundaries (except bone interfaces) with the shape of the surface mesh after deformation.

3.3. Thickness Computation

The thickness computation algorithm we propose evaluates the thickness values at every node of the surface mesh of cartilage. It is a 3D method which is independent of the orientation of the scan. The steps of the algorithm can be itemized as follows.

1. Construct the surface mesh of the cartilage, $\mathcal{M}$.

2. Separate $\mathcal{M}$ into two parts, top and bottom surfaces, $\mathcal{M}_t$ and $\mathcal{M}_b$, respectively.

3. Treat each surface as a deformable model and minimize their energy. For $\mathcal{M}_t$ ($\mathcal{M}_b$), $\mathcal{M}_b$ ($\mathcal{M}_t$) generates the external energy (target surface).

4. The thickness at node n_i is defined as the distance between pre and post deformation locations of n_i.

The separation of tibial cartilage surface mesh into top and bottom surfaces is achieved by considering the fact that a relatively flat object in 3D has a scattering matrix whose one of eigenvalues is considerably smaller than the other two. The plane of two principal axes which correspond to two greater eigenvalues approximates the flat object well. Thus, the normals of the opposed surfaces of the flat object point to different sides of that plane. These facts lead to a quite simple algorithm which investigates the angle between the normal and principal axis corresponding to smallest eigenvalue to decide the surface on which a particular node is located.

The separation of femoral cartilage is slightly more complicated than that of tibial cartilage due to the curved shape it possesses. However, femoral cartilage retains the properties of being flat and thin, locally. Hence, we separated it into top and bottom surfaces by dividing the bounding box of femoral cartilage into subvolumes in which the patches of femoral cartilage will be flat and thin and applying the above algorithm directly.

The energy definition of the deformable model we use for thickness computation purpose is identical to Eqns 3, 4, 13. However, the definition of $d(\mathbf{p}_i)$ is different from previous section. Since both the deformable surface and the target surface are defined on 3D continuous space, $d(\mathbf{p}_i)$ for $n_i \in \mathcal{M}_t$ is defined as follows:

$$d(\mathbf{p}_i) = \min_{n_j \in \mathcal{M}_b} \{\|\mathbf{p}_i - \mathbf{p}_j\|\} \tag{15}$$

We again use a greedy algorithm to to solve the minimization problem. The formulation of the energy term contributed by the node n_i is identical to Eqn 14. Recall that, the problem of minimizing $E(n_i)$ was solved using Powell's method in the previous section. However, the higher computational cost of evaluating $d(\mathbf{p}_i)$ in this framework makes utilization of Powell's method inefficient. We find the solution of Eqn 15 using brute force search which is significantly burdensome than bilinear interpolation. Due to this reason, we utilized the well-known Newton-Raphson method, a more direct approach than Powell's method, for solving the minimization problem.[19] It is solved iteratively as follows:
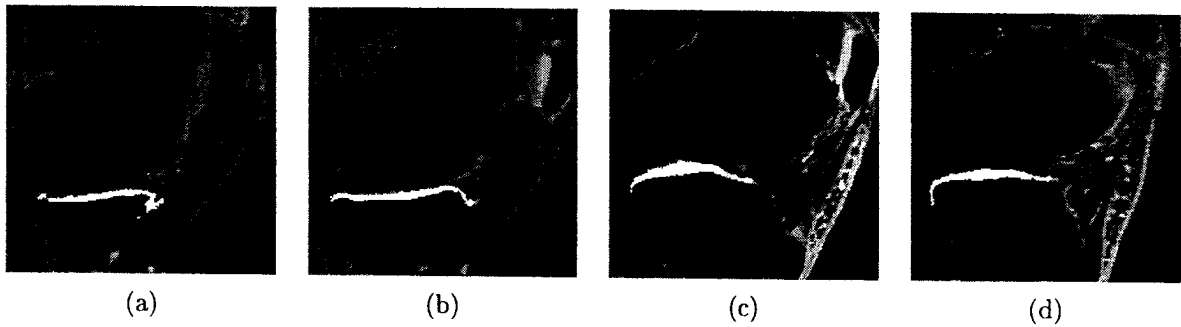
$$\mathbf{p}_i^{k+1} = \mathbf{p}_i^k - \mathbf{H}^{-1} \nabla E(n_i)|_{\mathbf{p}_i^k} \tag{16}$$

where k stands for the iteration number. $\nabla E(n_i)$ is the gradient of $E(n_i)$, and $\mathbf{H}$ is the Hessian matrix of $E(n_i)$, which is equal to

$$\mathbf{H} = \frac{d^2(d^2(\mathbf{p}_i))}{d\mathbf{p}_i^2} + 2 \left(\sum_{j \in \mathcal{N}_i} k_{ij} \right) \mathbf{I} \tag{17}$$

provided that $p_{xi} \neq p_{xj}$, $p_{yi} \neq p_{yj}$, and $p_{zi} \neq p_{zj}$, $\forall j$. $\mathbf{I}$ is a 3×3 identity matrix. With these definitions, thickness computation algorithm can be stated as follows:

Figure 2. The final segmentation result of tibial and femoral cartilages. The tibial and femoral cartilages are shaded with white and black, respectively. (a), (b), (c), (d) are the 17th, 20th, 42th, and 47th slices of the 3D volume, respectively.

ALGORITHM : THICKNESS COMPUTATION

$l = 1$
do
       for $\forall n_i \in \mathcal{M}_t$, $i = 1 \cdots N$
              Solve $\mathbf{p}_i^l = \arg\min_{\mathbf{p}_i} \left\{ E^l(n_i) \right\}$ using Newton-Raphson method
       end
       Compute $E^l(\mathcal{M}_t)$
       Increment l
while $\left| E^l(\mathcal{M}_t) - E^{l-1}(\mathcal{M}_t) \right| < \gamma_{tol,thk}$
for $\forall n_i \in \mathcal{M}_t$, $i = 1 \cdots N$
       $t(n_i) = \|\mathbf{p}_i^f - \mathbf{p}_i^0\|$

The superscript l denotes the iteration number. The thickness value at i^{th} node of $\mathcal{M}_t$ is denoted as $t(n_i)$. It is equal to the distance between points $\mathbf{p}_i^0$ and $\mathbf{p}_i^f$ which are the locations of the ith node prior to and after deformation of $\mathcal{M}_t$, respectively. Note that, the algorithm above computes the thickness values at the nodes of top surface only. For the nodes of bottom surface, same algorithm is used by changing $\mathcal{M}_t$ to $\mathcal{M}_b$.
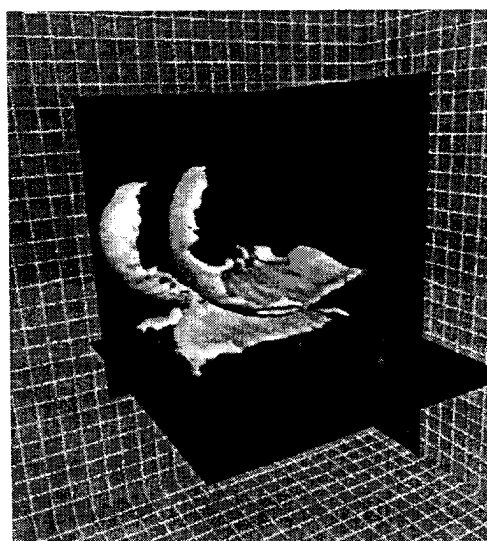
4. RESULTS

4.1. Cartilage Segmentation

An MRI scan of the knee whose size is $60 \times 175 \times 170$ is used to demonstrate the performance of the algorithm. The results of cartilage segmentation and separation of tibial and femoral cartilages can be seen in Figure 2 in which the 17th, 20th, 42th, and 47th slices are displayed. Furthermore, the 3D surface reconstruction of tibial and femoral cartilages are displayed in Figure 3. The cartilage surface is combined with three saggital, coronal, and axial slices from the MRI scan. We have compared the result of our cartilage segmentation algorithm with the manual tracing results performed by a radiologist. The comparison yielded accuracy, sensitivity, and specificity results, 98.87%, 66.22%, and 99.56%, respectively, considering the voxel labeling process as a binary hypothesis problem.

4.2. Thickness Computation

The performance of the thickness computation algorithm is analyzed on synthetic phantoms. We constructed two synthetic 3D objects whose surfaces are analytical functions. Thus, the exact thickness values of the objects are known. The bottom surfaces of both objects are flat at $z = f(x,y) = 0$. The top surface of the first phantom is a sinusoidal function whose formulation is given as:

$$f_1(x,y) = 5\sin(0.1(x - 50))\sin(0.1(y - 50)) + 30 \tag{18}$$

Figure 3. The surface reconstruction result of cartilage along with 13th, 109th, 25th, saggital, coronal, and axial slices, respectively.

The top surface of the second phantom is basically a 2D Gaussian modulated with the sinusoidal function in $f_1(x,y)$. It is given as:

$$f_2(x,y) = 5 \left(\exp(-r^2/2\sigma^2)\right)^{(r/5\sigma)^4} \sin(0.1(x-50))\sin(0.1(y-50)) + 30 \qquad (19)$$

where $r^2 = (x-125)^2 + (y-125)^2$ and $\sigma = 13$.

The cross-sections and the gray-scale maps of thickness distributions of both phantoms are depicted in Figure 4. We computed the thickness values at the nodes that belong to top or bottom surfaces. In Table 1, the performance of the algorithm is displayed by comparing its results to the analytical values. Note that, the top surfaces of the phantoms are essentially sinusoidals with 10 peak-to-peak units and a DC value of 30 units. The error values provided in Table 1 should be compared to the peak-to-peak value of the top surface without considering the DC value. According to this, the algorithm results in 1.9% and 0.8% RMS errors for first and second phantoms, respectively.
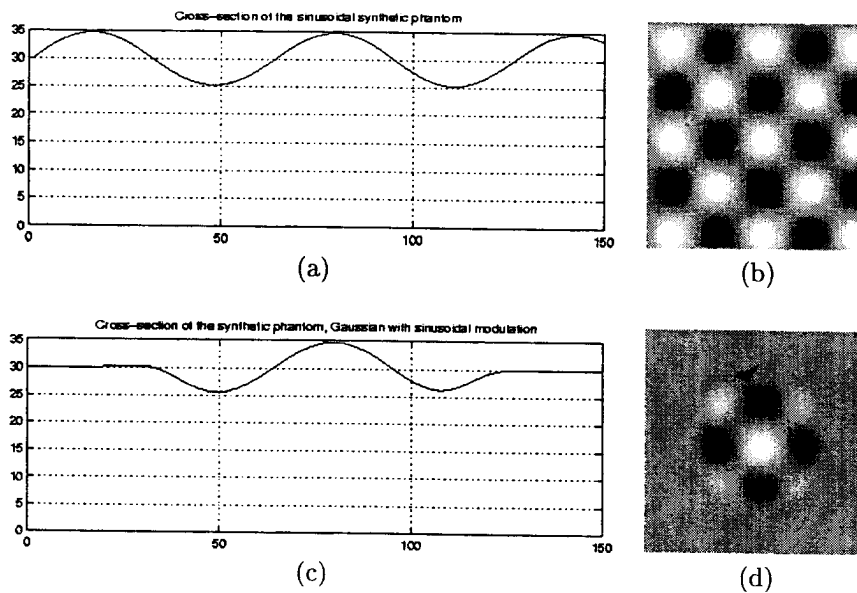
	Phantom 1		Phantom 2	
	Analytical	Experimental	Analytical	Experimental
mean	29.99	29.93	29.89	29.89
max	35.00	34.91	34.99	34.84
min	25.00	25.14	25.34	25.44
max. error	0.98		0.54	
avg. error	0.12		0.04	
RMS error	0.19		0.08	

Table 1. The results of the thickness computation experiments using theoretical 3D objects.

The thickness computation results of tibial and femoral cartilages are displayed at Figure 5 by mapping the thickness values to gray-scale. Furthermore the number of nodes in surface mesh, minimum, maximum, mean, median, and standard deviation of thickness values of both tibial and femoral cartilages are presented in Table 2.

5. CONCLUSIONS AND FUTURE WORK

In this paper, we have proposed unsupervised techniques for segmentation, surface reconstruction, and thickness computation of articular cartilage. The segmentation method is a mixture of region-growing, labeling and deformable models-type algorithms. The surface reconstruction provides sub-voxel accuracy by taking the MR imaging model

Figure 4. (a),(b) The cross-sections of the synthetic phantoms used for validation of thickness computation algorithm. (c), (d) The thickness values of the phantoms are mapped to gray-scale where white and black correspond to largest and smallest values, respectively. Phantom with top surface $f_1(x,y)$ and phantom with top surface $f_2(x,y)$ are displayed in c, and d, respectively.

|	Num. of nodes	min	max	mean	median	std
Femoral Cart.	28504	0.18	2.90	1.43	1.44	0.49
Tibial Cart.	14070	0.14	4.11	1.44	1.30	0.75

Table 2. The results of tibial and femoral cartilage thickness computation (mm).

into account. The thickness computation algorithm we propose results in thickness values that are independent of scan orientation and displayed in the form of a grayscale map.

The future work on this subject consists of the validation study which is already an ongoing effort. Specifically, the thickness maps of 10 rabbit cartilages which include 5 healthy and 5 arthritis cases will be constructed. The validity of the algorithms will be investigated by comparing the results to the histology studies.

REFERENCES

1. S. Solloway, C. E. Hutchinson, J. C. Waterton, and C. J. Taylor, "The use of active shape models for making thickness measurements of articular cartilage from mr images," *Magnetic Resonance in Medicine* **37**, pp. 943–952, 1997.
2. T. F. Cootes, C. J. Taylor, D. H. Cooper, and J. Graham, "Active shape models - their training and application," *Computer Vision and Image Understanding* **61**, pp. 38–59, 1995.
3. F. Eckstein, M. Schnier, M. Haubner, J. Priebsch, C. Glaser, K. H. Englmeier, and M. Reiser, "Accuracy of cartilage volume and thickness measurements with magnetic resonance imaging," *Clinical Orthopaedics and Related Reserach* **352**, pp. 137–148, 1998.
4. T. Stammberger, F. Eckstein, M. Michaelis, K. H. Englmeier, and M. Reiser, "Interobserver reproducibility of quantitative cartilage measurements: Comparison of b-spline snakes and manual segmentation," *Magnetic Resonance Imaging* **17**, pp. 1033–1042, 1999.
5. T. Stammberger, F. Eckstein, K. H. Englmeier, and M. Reiser, "Determination of 3d cartilage thickness data from mr imaging: Computational method and reproducibility in the living," *Magnetic Resonance in Medicine* **41**, pp. 529–536, 1999.

<div align="center">(a)   (b)</div>
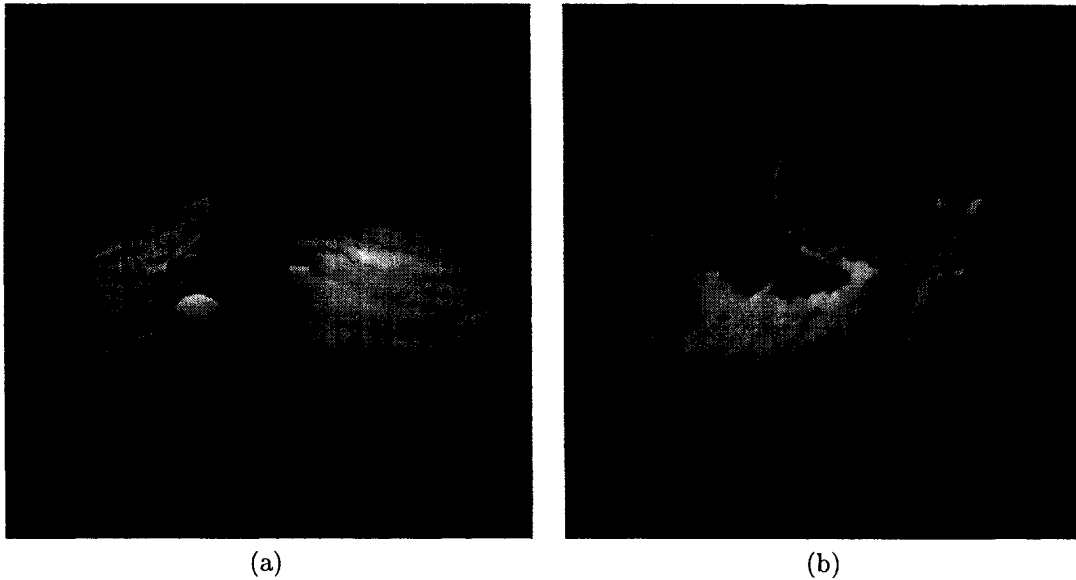
Figure 5. The surface reconstruction of tibial and femoral cartilages. The thickness values at each node of the surface meshes are mapped to gray-scale. According to this, for each surface, minimum thickness and maximum thickness are mapped to black and white, respectively. The minimum and maximum values corresponding to both surfaces can be seen in Table 2.

6. J. G. Tamez-Pena, *Four-Dimensional Reconstruction and Visualization of Complex Musculoskeletal Structures*, Ph.D. Thesis, Univ. of Rochester, 1999.

7. S. K. Pakin, R. S. Gaborski, L. Barski, D. H. Foos, and K. J. Parker, "Segmentation of bone and soft tissue regions in digital radiographic images of extremities," in *Proceedings of SPIE, Medical Imaging 2001: Image Processing, vol. 4322, pp 1296-1302*, San Diego, CA, 2001.

8. P. Danielsson, "Eucledian distance mapping," *Computer Graphics and Image Processing* **14**, pp. 227-248, 1980.

9. O. Cuisenaire and B. Macq, "Fast eucledian distance transformation by propagation using multiple neighborhoods," *Computer Vision and Image Understanding* **76**, pp. 163-172, 1999.

10. S. A. Hojjatoleslami and J. Kittler, "Region growing; a new approach," *IEEE Trans. on Image Proc.* **7**, pp. 1079-1084, 1998.

11. M. Kaas, A. Witkin, and D. Terzopoulos, "Snakes: Active contour models," *International Journal of Computer Vision* **1**, pp. 321-331, 1988.

12. I. Cohen, L. D. Cohen, and N. Ayache, "Using deformable surfaces to segment 3-d images and infer differential structures," *CVGIP: Image Understanding* **56**, pp. 242-263, 1992.

13. H. Eviatar and R. L. Somorjai, "A fast, simple active contour algorithm for biomedical images," *Pattern Recognition Letters* **17**, pp. 969-974, 1996.

14. N. E. Davison, H. Eviatar, and R. L. Somorjai, "Snakes simplified," *Pattern Recognition* **33**, pp. 1651-1664, 2000.

15. P. L. George and H. Borouchaki, *Delaunay Triangulation and Meshing*, Hermes, 1998.

16. W. Schroeder, K. Martin, B. Lorensen, W. Schroeder, and W. E. Lorensen, *The Visualization Toolkit*, Prentice Hall, 1997.

17. G. A. Wright, "Magnetic resonance imaging," *Signal Processing* , pp. 56-66, 1997.

18. D. J. Williams and M. Shah, "A fast algorithm for active contours and curvature estimation," *CVGIP: Image Understanding* **55**, pp. 14-26, 1992.

19. W. H. Press, S. A. Teukolsky, W. T. Vetterling, and B. P. Flannery, *Numerical Recipes in C*, Cambridge University Press, 1992.